Groove Stiffening of Sheets by Single Point Incremental Forming

Journal:	*Part B: Journal of Engineering Manufacture*
Manuscript ID	JEM-22-0391.R1
Manuscript Type:	1st International Conference on Engineering Manufacture 2022 (EM 2022)
Date Submitted by the Author:	n/a
Complete List of Authors:	Cristino, Valentino; University of Macau, Department of Electromechanical Engineering Pragana, João; Universidade de Lisboa Instituto Superior Tecnico, Mechanical Engineering Bragança, Ivo; Instituto Politécnico de Lisboa Instituto Superior de Engenharia de Lisboa, Mechanical Engineering Silva, Carlos; Universidade de Lisboa Instituto Superior Tecnico, Mechanical Engineering Martins, Paulo; Universidade de Lisboa Instituto Superior Tecnico, Mechanical Engineering
Keywords:	Single point incremental forming, Stiffening grooves, Analytical framework, Finite element method, Experimentation
Abstract:	This paper investigates the applicability of single point incremental forming to fabricate stiffening grooves in thin metallic panels. The work combines experimentation, finite element, and analytical modelling to determine the required forces and the maximum allowable groove depths that can be produced without tearing. The analytical modelling is based on a framework that was previous developed by the authors and combines in-plane membrane stretching and fracture forming limits. Comparison of the results obtained by the analytical framework against experimental and finite element data prove its effectiveness to replicate the deformation mechanics of groove stiffening by single point incremental forming. Results also prove that groove stiffening by single point incremental forming is an easy and effective alternative to conventional reinforcement of thin metallic panels by welding or fastening of stringers.

GROOVE STIFFENING OF SHEETS BY SINGLE POINT INCREMENTAL FORMING

Valentino A.M. Cristino[a], João P.M. Pragana[b], Ivo M.F. Bragança[c], Carlos M.A. Silva[b], Paulo A.F. Martins[b,]*

[a]Department of Electromechanical Engineering, University of Macao, Avenida da Universidade, Taipa, Macao
[b]IDMEC, Instituto Superior Técnico, Universidade de Lisboa, Portugal
[c]CIMOSM, Instituto Superior de Engenharia de Lisboa, Instituto Politécnico de Lisboa, Portugal

First author. E-mail: vcristino@um.edu.mo
Second author. E-mail: joao.pragana@tecnico.ulisboa.pt
Third author. E-mail: ibraganca@dem.isel.ipl.pt
Fourth author. E-mail: carlos.alves.silva@tecnico.ulisboa.pt
Corresponding author. E-mail: pmartins@tecnico.ulisboa.pt Telephone: +351218419006

ABSTRACT

This paper investigates the applicability of single point incremental forming to fabricate stiffening grooves in thin metallic panels. The work combines experimentation, finite element, and analytical modelling to determine the required forces and the maximum allowable groove depths that can be produced without tearing. The analytical modelling is based on a framework that was previous developed by the authors and combines in-plane membrane stretching and fracture forming limits. Comparison of the results obtained by the analytical framework against experimental and finite element data prove its effectiveness to replicate the deformation mechanics of groove stiffening by single point incremental forming. Results also prove that groove stiffening by single point incremental forming is an easy and effective alternative to conventional reinforcement of thin metallic panels by welding or fastening of stringers.

Keywords: Single Point Incremental Forming; Stiffening Grooves; Analytical Framework; Finite Element Method; Experimentation

1. INTRODUCTION

Stretch forming is a metal forming process commonly used in aeronautic, automotive, naval and building sectors that simultaneously stretches and bends thin metal sheets over a punch to produce smooth, curved, panels with different surfaces and thicknesses[1] (Figure 1a). These panels (hereafter referred to as 'thin panels') are often reinforced with stringers that are welded or fastened (by means of rivets or bolts) to their surfaces.

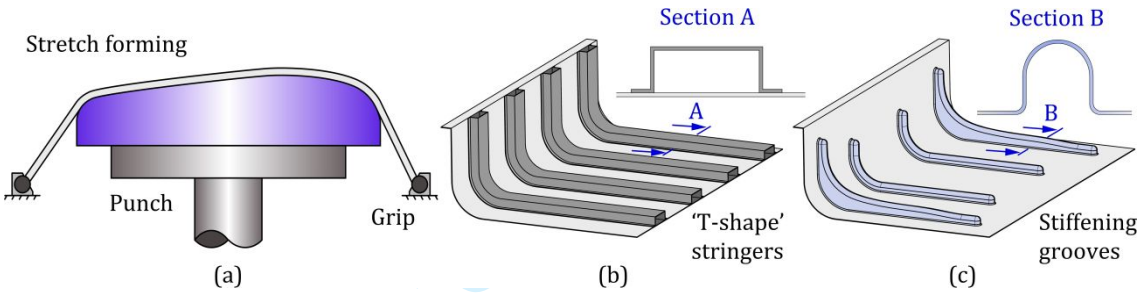

Figure 1 (a) Stretch forming of thin panels and strengthening by means of longitudinal (b) 'T-shape' stringers or (c) stiffening grooves.

The alternative of using stringers to reinforce thin panels before stretch forming is usually not an option due to the possibility of cracking and buckling caused by tension and compression loadings during plastic deformation. To make this alternative viable for industrial implementation, Köhler et al.[2] recently proposed a solution based on a cam-actuated mechanism that can assemble the stringers on the panels before stretch forming. The solution successfully prevents the occurrence of buckling by providing lateral support of the stringers during stretch forming but gives rise to other types of failure plus substantial elastic recovery. It also increases the complexity and cost of the tools and manufacturing routes, when compared to existing solutions based on conventional stretching and reinforcement by welding or fastening.

Resort to manufacturing solutions where the panels and reinforcements are milled from a single billet, allows producing thin monolithic (homogeneous), lightweight panels with integrated stringers that are easy and cost effective to assemble. In fact, thin monolithic panels eliminate the use of rivets or screws as well as the metallurgical changes in the heat-

affected zones and the thermal-induced distortions resulting from welding that lead to difficulties in obtaining the desired geometry and performance of the panels.

The main drawbacks associated to the fabrication of thin monolithic panels by milling are the final surface roughness, the overall machining time, and the big waste of material, which can account for more than 95% of the initial billet[3]. Still, this type of panels is commonly used in aeronautics[4].

Roll forming allows overcoming some of the disadvantages of milling, but its use is limited to large batch production of thin monolithic panels having a uniform profile throughout the surface (for example, the motorway metallic rails). Over-bending in the open section of the panels may also diminish their overall quality and trigger other defects such as edge wrinkling[5].

Other manufacturing solutions based on conventional forming of grooves with punch and die sets[6,7] are limited by the time and cost to fabricate the tools and because these are dependent on the geometry of the panels. Despite electromagnetic forming allows one element of the tool set (usually the punch) to be replaced by a coil, this process variant is limited to highly conductive materials, to small size panels and cannot avoid the groove geometry dependence of the dies[8].

This paper explores the potential of single-point incremental forming (SPIF) to locally emboss stiffening grooves in thin panels using a single clamping (Figure 1c) as it was originally proposed by Slota et al.[9] and previously utilized by Lu et al.[10] to evaluate friction between the forming tool and panels. The possibility of performing the forming and stiffening stages simultaneously combined with the dieless characteristics of SPIF[11], leads to greater flexibility and economic benefits than those currently offered by conventional reinforcement by stringers.

The work to be presented combines experimentation, finite element analysis and theoretical modelling using an analytical framework previous developed by the authors[12],

to determine the required forming forces and the maximum allowable groove depths that can be produced without tearing.

2. MATERIALS AND METHODS

2.1 Mechanical characterization

The work was carried out in AISI 316L stainless steel sheets with 1 mm thickness. The mechanical properties and flow curve of the material were determined by means of tensile tests on an INSTRON 5900 universal testing machine, according to the ASTM standard E8/E8 M-16[13]. The specimens were cut out from the supplied sheets at 0°(P-parallel), 45°(I-inclined) and 90°(T-transversal) inclination with respect to the rolling directions and Figure 2 and Table 1 summarize the results obtained from these tests.

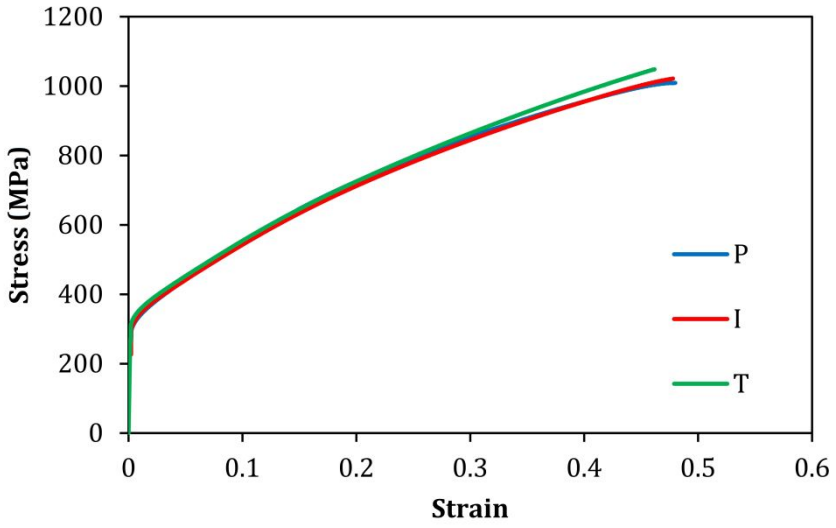

Figure 2 True stress–strain curves of AISI 316L stainless steel sheets. The symbols P, I and T refer to the parallel, inclined, and transverse orientations against the rolling direction.

Table 1. Mechanical properties of the AISI 316L stainless steel sheets.

Material	Orientation	Yield stress (MPa)	Elongation at break (%)	Anisotropy coefficient
AISI 316L	P	320.7 ± 4.4	64.9 ± 3.3	0.94
	I	313.5 ± 3.1	63.6 ± 3.5	0.97
	T	310.5 ± 3.8	61.2 ± 4.1	0.98
Average values		312.25	63.33	0.97

2.2 Experimentation

Groove stiffening by SPIF was carried out in sheet specimens with a geometry of 130 mm x 50 mm x 1 mm. The experimental setup to fabricate the stiffening grooves is shown in Figure 3. and consists of: (a) a forming tool with a semi-hemispherical tip of 6 mm radius, made from a cold working alloy tool steel with chromium, vanadium, and tungsten (120WV4—DIN), hardened and tempered to 60 HRC; (b) a backing plate and (c) a screw-loaded pressure pad located at the outer perimeter of the sheet.

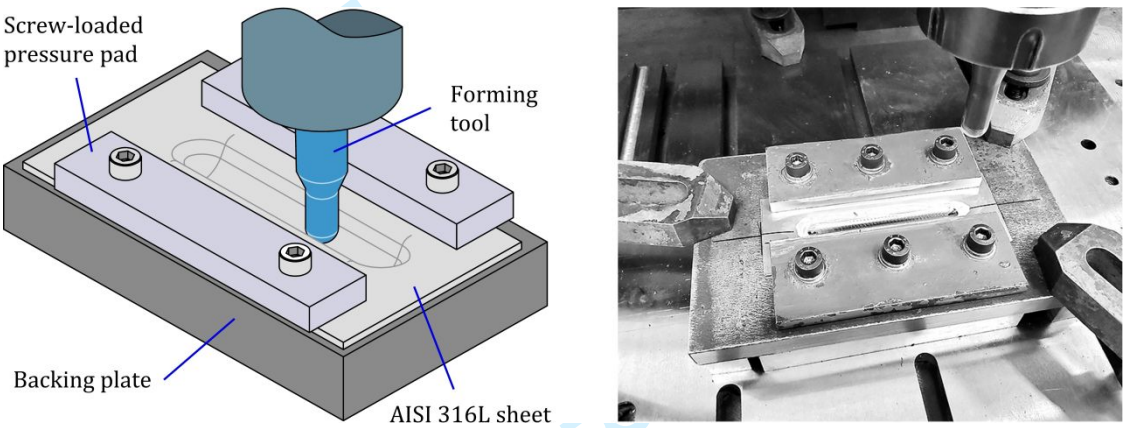

Figure 3 Schematic representation and photograph of the experimental setup to fabricate the stiffening grooves by SPIF under laboratory conditions.

SPIF was carried out with a straight alternating longitudinal path and a vertical step size of 1 mm. The feed rate and rotation speeds were equal to 200 mm/min and 100 rpm, respectively.

A ceramic grease Weicon ASW 040P was applied on the tool-sheet interface for lubrication. All the sheet specimens were electrochemically etched with a grid of overlapping circles having an initial diameter of 2 mm for allowing measuring the major and minor axis of the ellipses and quantifying the in-plane strains (ε_ϕ,ε_z) resulting from plastic deformation of the circles (a procedure known as 'circle grid analysis'[14]). The measurements were performed for various groove depths H with a computer-aided system consisting of a 3Com USB camera and the GPA 3.0 software.

2.3 Finite element analysis

Finite element simulation of groove stiffening by SPIF was carried out with the commercial software LS-DYNA. The sheet specimens were modelled as elastic-plastic deformable objects and discretized by means of adaptive meshes consisting of 6500 shell elements with approximately 1 mm x 1 mm initial size and five integration points through thickness (Figure 4). The semi-hemispherical tip forming tool and the backing plate were modelled as rigid objects and the tool moving path was set identical to that of the actual SPIF process.

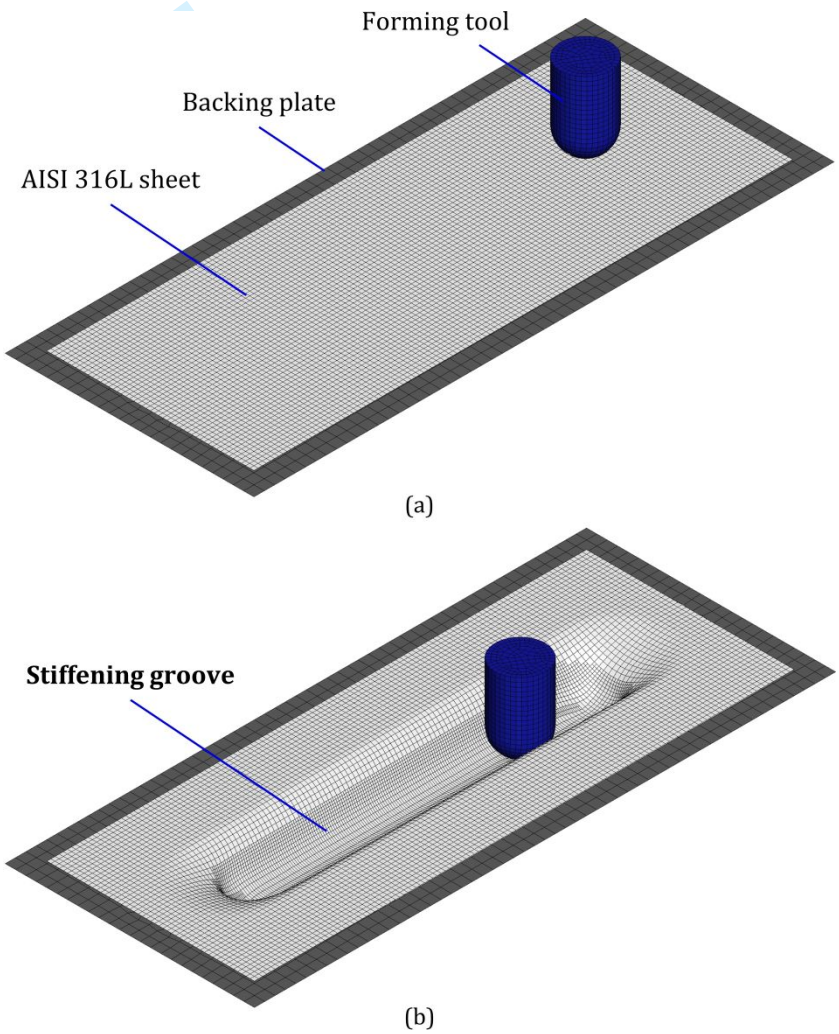

Figure 4 (a) Initial and (b) final computed meshes obtained from finite element analysis.

The AISI 316L stainless-steel sheet specimens were assumed as isotropic ($r \cong 1$) and material strain hardening was characterized by means of an average Hollomon power law resulting from the tensile tests performed in different directions (Table 1).

The simulations were performed with a load factoring (or time-scaling) procedure to reduce the overall CPU time, which was approximately equal to 5 hours in a computer equipped with an Intel i7-6700 (3.4 GHz) processor.

2.4 Analytical framework

Experimental observations (refer to Section 3) of groove stiffening by SPIF showed that material deforms under plane strain loading conditions ($\beta = d\varepsilon_z/d\varepsilon_\phi = 0$), except at the entry and exit of the tool during which material flows under biaxial stretching loading conditions ($\beta = d\varepsilon_z/d\varepsilon_\phi = 1$). The analytical framework to be presented in this section is limited to steady-state, plane-strain conditions.

Figure 5 presents a schematic cross-section of a stiffening groove, which consists of a membrane subjected to in-plane stretching (i.e., without bending moments). Three-main regions can be identified in Figure 5a: (i) the contact angle θ around the forming tool, (ii) the straight unsupported length L_s with an angle α_s against the forming tool center and (iii) the curvature radius R_b of the backing plate.

The contact angle θ around the forming tool is given by,

$$\theta = \frac{\pi}{2} - \alpha_s - \alpha_b \tag{1}$$

where the angles α_s and α_b are shown in Figure 5a and are related with the radius of the forming tool R, and the groove depth H and width W, as follows,

$$\alpha_b = arctan\left(\frac{R - H + R_b}{W}\right) \tag{2}$$

$$\alpha_s = arccos\left(\frac{R_b + R}{\sqrt{\{W^2 + (R - H + R_b)^2\}}}\right) \tag{3}$$

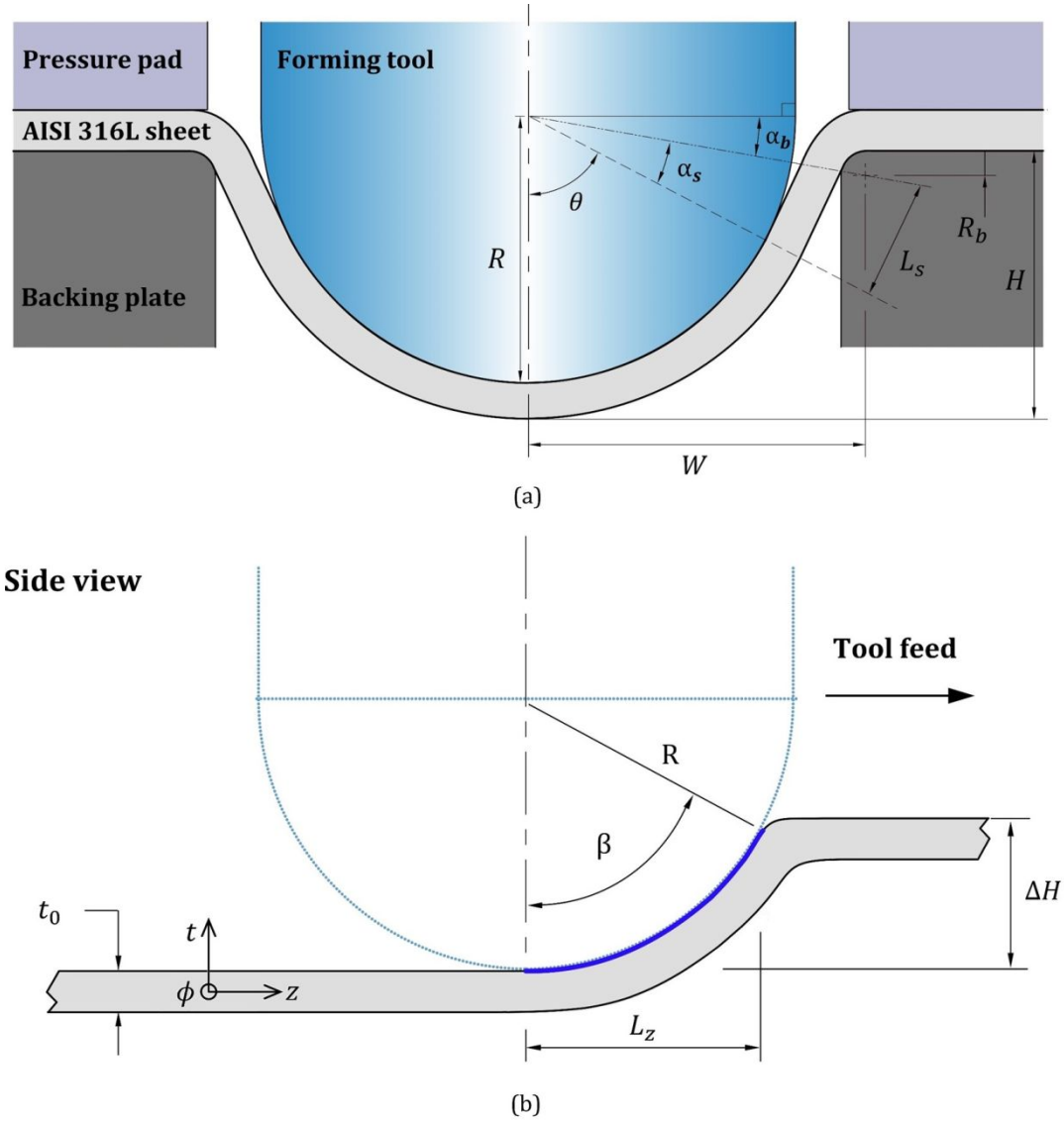

Figure 5 (a) Cross-section of the stiffening groove with notation; (b) Area of the local contact between the tool and the sheet placed immediately ahead.

The meridional (ϕ), thickness (t) and longitudinal (z) directions are assumed as principal directions subjected to plane stress $\sigma_t = 0$ loading along the thickness direction, as it is commonly assumed in sheet metal forming.

Average meridional strain

The material of the sheet specimens is assumed as isotropic (Table 1) and rigid plastic with strain hardening according to the Hollomon relationship $\bar{\sigma} = k\bar{\varepsilon}^n$. Under these conditions,

the effective strain $\bar{\varepsilon}$ along the stiffening groove perimeter and the corresponding meridional stress σ_ϕ can be directly obtained from the meridional strain ε_ϕ as follows,

$$\bar{\varepsilon} = \frac{2}{\sqrt{3}}\varepsilon_\phi$$
$$\sigma_\phi = \frac{2}{\sqrt{3}}\bar{\sigma} \tag{4}$$

The meridional strain ε_ϕ in (4) can be determined from experimental circle grid analysis, finite element simulation and from the analytical framework under consideration. In case of the latter, it requires determining the evolution of L_ϕ with depth H during stretching following a procedure like that earlier proposed by Martins and Marques[15] for stretch forming with a cylindrical punch.

$$L_\phi = (R + R_b)\theta + L_s \tag{5}$$

In the above equation the length L_s is given by,

$$L_s = \sqrt{\{W - (R + R_b)sin\theta\}^2 + \{H - (R + R_b)(1 - cos\theta)\}^2} \tag{6}$$

where W is the original (undeformed) sheet length from where the groove is plastically formed.

Under these circumstances, the average value of the meridional strain ε_ϕ^{avg} in the groove is obtained from,

$$\varepsilon_\phi^{avg} = ln\left(\frac{L_\phi}{W}\right) \tag{7}$$

Forming force

The forming force F necessary for the fabrication of stiffening grooves by SPIF is determined from,

$$F = 2\sigma_{\phi}^{avg} t_0 L_z sin\theta exp\left(-\varepsilon_{\phi}^{avg}\right) \tag{8}$$

where t_0 is the initial thickness, L_z is the contact length between the tool and the sheet placed immediately ahead (Figure 5b) and σ_{ϕ}^{avg} is the average meridional stress. The later can be determined from the increments of average meridional strain $d\varepsilon_{\phi}^{avg}$ as follows,

$$\sigma_{\phi}^{avg} = \frac{4\,\overline{\sigma}}{3d\overline{\varepsilon}} d\varepsilon_{\phi}^{avg} \tag{9}$$

Maximum allowable groove depth

The maximum allowable groove depth is determined by combining the average meridional strain ε_{ϕ}^{avg} (7) with the Levy-Mises constitutive equations under plane strain ($\varepsilon_z = 0$) and plane stress ($\sigma_t = 0$) combined conditions,

$$\begin{aligned} d\varepsilon_{\phi} &= \frac{1 d\overline{\varepsilon}}{2\,\overline{\sigma}}[2\sigma_{\phi} - \sigma_z] \\ d\varepsilon_z &= \frac{1 d\overline{\varepsilon}}{2\,\overline{\sigma}}[2\sigma_z - \sigma_{\phi}] = 0 \\ d\varepsilon_t &= \frac{1 d\overline{\varepsilon}}{2\,\overline{\sigma}}[-\sigma_z - \sigma_{\phi}] \end{aligned} \tag{10}$$

This procedure allows relating the average thickness strain ε_t^{avg} and the average longitudinal stress σ_z^{avg} with the corresponding meridional values, as follows,

$$\varepsilon_t^{avg} = -\varepsilon_\phi^{avg} \tag{11}$$

$$\sigma_z^{avg} = \frac{1}{2}\sigma_\phi^{avg} \tag{12}$$

and determining the average thickness t^{avg} of the groove by means of,

$$t^{avg} = t_0 exp\left(-\varepsilon_t^{avg}\right) \tag{13}$$

Determination of the maximum allowable groove depth H_{max} starts by assuming that the force per unit of length $T_\phi = \sigma_\phi t$ in the meridional direction is constant. This assumption earlier employed by Cristino et al.[12] considers material strain hardening to balance reduction in thickness and is widely employed in sheet metal forming modelling[16].

Under these assumptions, T_ϕ can be determined by combining equations (9) and (13),

$$T_\phi = \sigma_\phi^{avg} t^{avg} = C \tag{14}$$

where C is a constant value for an arbitrary groove depth H.

The fracture forming limit (FFL) of the AISI 316L sheets in principal strain space was previously determined by the authors[12] and allows identifying the critical meridional strain ε_ϕ^{crit} at the onset of cracking. This enables obtaining the minimum sheet thickness t_{min} by employing equation (13) for critical values instead of average values,

$$t_{min} = t_0 exp\left(-\varepsilon_t^{crit}\right) \qquad \varepsilon_t^{crit} = -\varepsilon_\phi^{crit} \tag{15}$$

Once the minimum sheet thickness t_{min} of the stiffening groove is obtained and the critical meridional stress σ_ϕ^{crit} is obtained by employing equation (9) for critical values, one can determine the critical force value per unit of length T_ϕ^{crit}, as follows,

$$T_{\phi}^{crit} = \sigma_{\phi}^{crit} t_{min} = C^{crit} \quad (16)$$

This last result can then be used to predict the maximum allowable groove depth H_{max}, which corresponds to the instant of time when T_{ϕ} (14) is equal to T_{ϕ}^{crit} (16) at the onset of tearing.

3. RESULTS AND DISCUSSION

3.1. Shape, thickness, and strain path evolutions

Figure 6a presents the experimental, finite element and analytical evolutions of the cross-sectional geometry of the stiffening groove for two different instants of time corresponding to values of depth H equal to 5 mm and 11 mm, respectively. Due to symmetry, only half of the cross-section is shown.

The overall agreement is good and the main differences between the analytical and the experimental and finite element results that are observed in Figure 6a are attributed to the elastic recovery of the stiffening grooves after unloading and halving the sheet specimens lengthwise to reveal their cross-sections and measuring the geometrical profile and thickness. In fact, the elimination of the circumferential constraint due to halving of the sheet specimens is not considered in the finite element simulation.

Figure 6b presents the same type of comparison for the thickness of the stiffening grooves. In this case, the main differences are observed between the analytical and the experimental and finite element results because the former can only provide average thickness t^{avg} (13) values for each groove depth H. However, as will be shown in what follows, this will not compromise the performance of the analytical framework for predicting the required forming force and the maximum allowable groove depth.

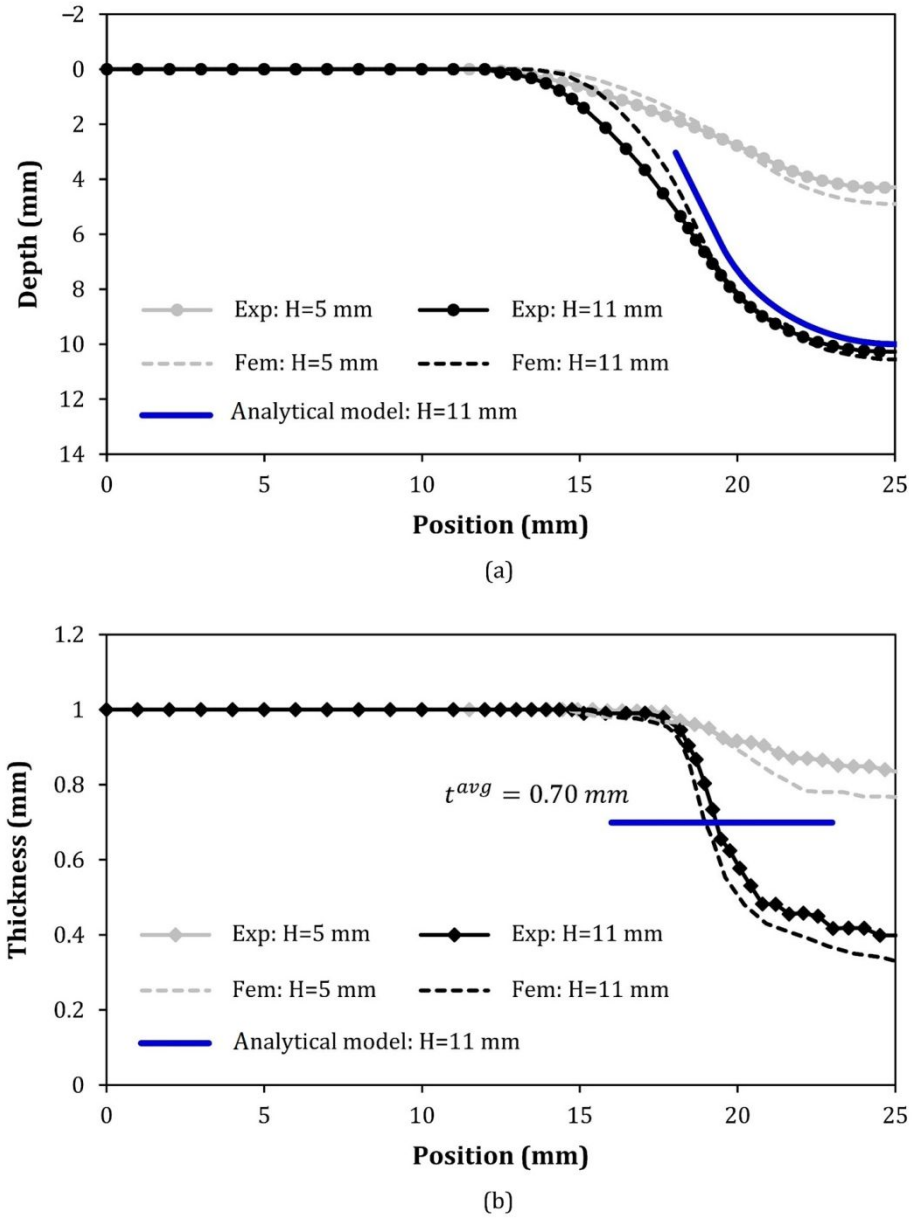

Figure 6 Experimental, numerical, and analytical evolutions of the (a) cross-sectional geometry and (b) thickness of the stiffening groove for two different instants of time corresponding to a groove depth H of the semi-hemispherical tip tool equal to 5 mm and 11 mm.

Figure 7 shows the experimentally measured and the finite element predicted evolutions of the in-plane meridional ε_ϕ and longitudinal ε_z strains along the perimeter of the groove for the instant of time after tearing of the sheet specimens by opening and propagation of cracks. As seen, the in-plane strains fall close to the vertical axis, in close agreement with the earlier assumption that material is subjected to plane strain deformation up to the onset of fracture. Moreover, because no signs of necking are observed in the grooves, as can also

be concluded from the observation of the evolution of thickness in Figure 6b, it may be stated that groove stiffening by single point incremental forming fails by critical thickness reduction and crack opening by tension (mode I of fracture mechanics) without previous necking[14].

After validating the shape and thickness obtained from analytical and finite element modelling against experimental values, attention will now be focused on determining the maximum allowable depts of the stiffening grooves and the required forming forces because this information is of paramount importance to the design and fabrication of thin reinforced panels.

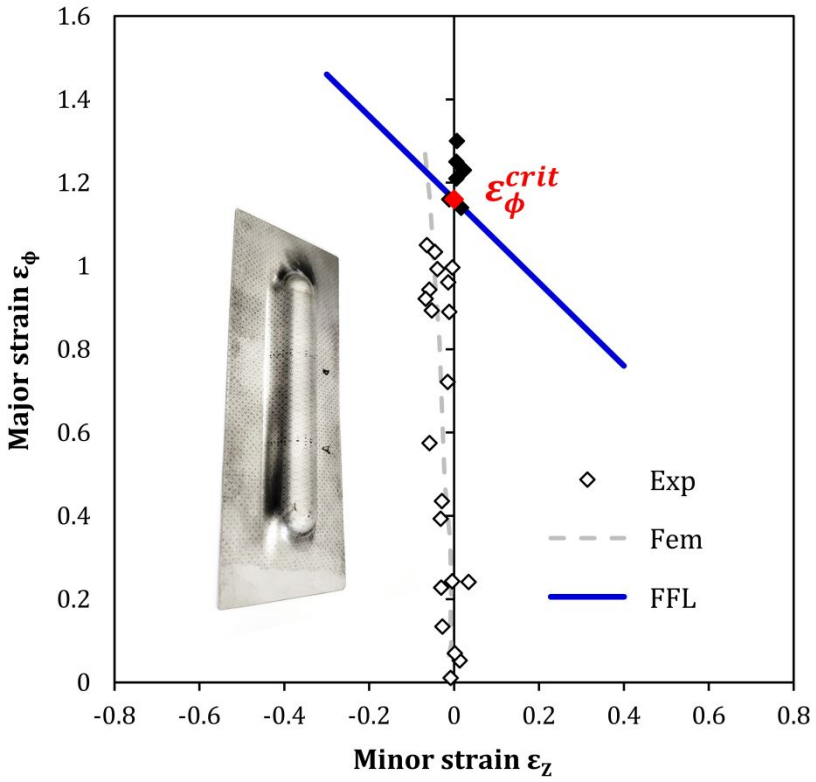

Figure 7 Principal strain space showing the experimental and finite element computed in-plane strains along the perimeter of the stiffening groove for an instant of time corresponding to a depth $H = 14$ mm immediately after cracking.

3.2. Maximum depth

Combining equations (14) and (4) with the Hollomon strain-hardening relationship $\bar{\sigma} = k\,\bar{\varepsilon}^n$ for average meridional strain ε_ϕ^{avg} values, it is possible to determine the analytical

evolution of the force per unit of length T_ϕ as a function of the stiffening groove depth H as follows,

$$T_\phi = \frac{2}{\sqrt{3}}\bar{\sigma}^{avg}t^{avg} = C(H) \qquad \text{with } \bar{\sigma}^{avg} = k\left(\frac{2}{\sqrt{3}}\varepsilon_\phi^{avg}\right)^n \tag{17}$$

The relation given by equation (17) is plotted in Figure 8 and the maximum allowable depth H_{max} is obtained by searching the point in the $T_\phi = C(H)$ evolution that matches the critical value C^{crit} (16) obtained from the onset of failure by fracture based on the critical meridional strain ε_ϕ^{crit} determined from the FFL (Figure 7). The procedure is illustrated in Figure 8 through the intersection between the $T_\phi = C(H)$ evolution and the red solid line corresponding to the critical values of T_ϕ^{crit}.

As seen, the maximum allowable depth H_{max} obtained from the analytical framework is similar to that predicted by finite elements and slightly above the experimentally measured $H_{max} = 14$ mm.

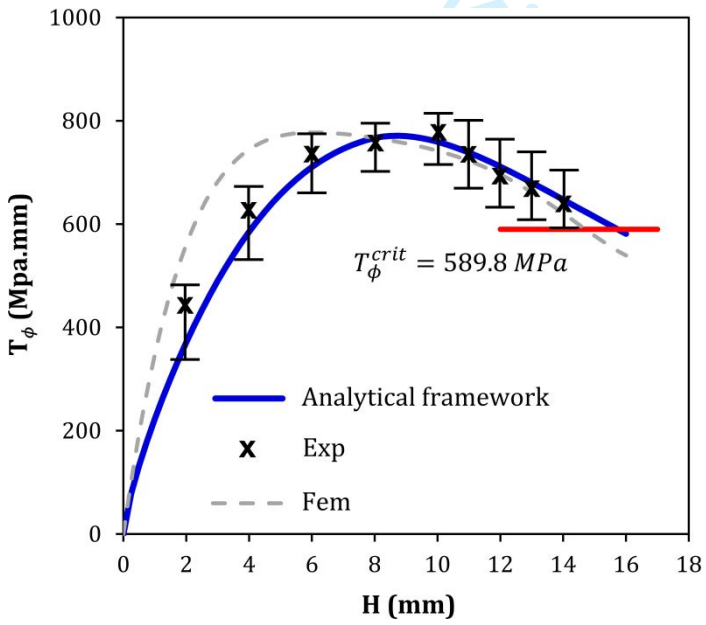

Figure 8 Force per unit of length as a function of the groove depth.

3.3. Forming tool force

Figure 9 shows the evolutions of the experimental, analytical, and numerical forming tool force F (8) with the groove depth H. As seen, while the predictions obtained by means of finite elements tend to overestimate the experimental values, those obtained from the analytical framework tend to underestimate them. Still, both numerical model and analytical framework can predict the overall force vs. depth evolution with differences in the latter being attributed to simplifying assumptions consisting of: (i) usage of average values instead of local values for the process main variables and (ii) uncertainty in establishing the contact length L_z (Figure 5b).

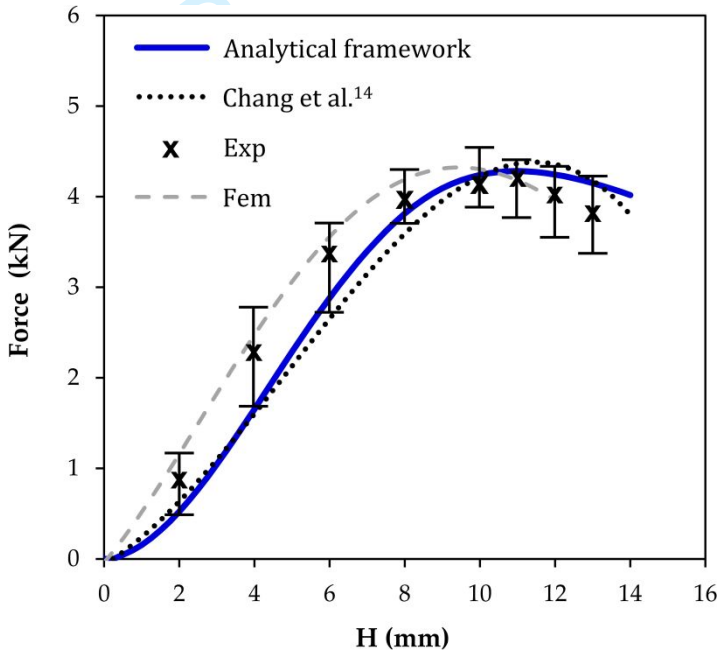

Figure 9 Experimental, numerical, and analytical evolutions of the forming tool force vs. groove depth.

Finally, the results provided by the new proposed analytical framework were compared against those obtained from a recently proposed analytical framework developed by Chang et al.[17]. This other analytical framework makes use of the instantaneous wall angle and thickness values for each value of groove depth, which need to be obtained beforehand from the experimental cross-section profiles (or, alternatively, from the corresponding finite element predictions) at different instants of time. However, despite the greater

completeness and complexity of this model, the predicted evolution of the forming force with depth is nearly identical to that given by the analytical framework described in this paper.

4. CONCLUSIONS

Groove stiffening of thin panels by single point incremental forming (SPIF) is an alternative solution to conventional reinforcement by means of welded or fastened stringers. This type of reinforcement avoids the need of assembling operations and additional joining elements and eliminates the thermal-induced metallurgical changes and deformations that risk achieving the final required geometry and performance of the panels.

SPIF subjects the thin panels to in-plane stretching, and the deformation mechanics of groove stiffening can be analytically described by in-plane stretching of a membrane. The proposed analytical framework is successfully utilized to determine the forming forces to produce the grooves and to estimate the maximum allowable groove depth before failure. Failure occurs by cracking along the longitudinal direction under opening mode I (by tension applied in the meridional directions).

Comparisons against experimental measurements, finite element estimates, and alternative analytical solutions prove the effectiveness, simplicity, and very fast obtention of results by means of the analytical framework that was previously developed by the authors.

ACKNOWLEDGMENTS

The authors would like to thank the support provided by Fundação para a Ciência e a Tecnologia of Portugal and IDMEC under LAETA-UIDB/50022/2020. Valentino A.M. Cristino would like to thank for the financial support of the University of Macau through the Start-up Research Grant SRG2019-00161-FST.

CONFLICT OF INTEREST:

The authors declare that they have no conflict of interest.

REFERENCES

1. Klocke, F. Manufacturing Processes 4 – Forming. Springer, Aachen, Germany, 2013: 332-339.
2. Köhler, S, Rohnert, C, Groche, P. Extension of geometric limits in drawing of stringer sheets. In (Eds. Mori KI, Abe Y, Maeno T) Proceedings of the 17th International Conference on Metal Forming - Metal Forming 2018, Toyohashi, Japan. Procedia Manufacturing 2018; 15: 693-700.
3. Shamsuddin, KA, Ab-Kadir, AR, Osman, MH. A comparison of milling cutting path strategies for thin-walled aluminium alloys fabrication. International Journal of Engineering and Science 2013; 2: 1-8.
4. Seguy, S, Campa, FJ, Lacalle, LNL, Arnaud, L, Dessein, G, Aramendi, G. Toolpath dependent stability lobes for the milling of thin-walled parts. International Journal of Machining and Machinability of Materials 2009; 4: 377-392.
5. Bidabadi BS, Naeini HM, Safdarian R. Investigation of over bending defect in the cold roll forming of U-channel section using experimental and numerical methods. Journal of Engineering Manufacture 2022; 236: 1380-1392.
6. Fusano, L, Priarone, PC, Avalle, M, Filippi, AM. Sheet metal plate design: a structured approach to product optimization in the presence of technological constraints. International Journal of Advanced Manufacturing Technology 2011; 56: 31-45.
7. Lacki, P, Adamus, J. Numerical analysis of forming sheet panels with stiffening ribs. In (Eds. Oñate E, Owen DRJ, Peric D, Chiumenti M) Proceedings of the 13rd. International Conference on Computational Plasticity. Fundamentals and Applications – COMPLAS XIII, Barcelona, Spain, CIMNE 2015: 204-215.

8. Eguia, I, Mangas, A, Iturbe, R, Gutiérrez, MA. Electromagnetic forming of longitudinal strengthening ribs in roll formed automotive profiles. In (Eds. Babusci K, Daehn G, Marré M, Tekkaya AE, Weddeling C, Zhang Y). Proceedings of the 4th International Conference on High-Speed Forming—ICHSF 2010, Columbus, USA, 2010: 200-207.
9. Slota, J, Kubit, A, Trzepiecinski, T, Krasowski, B, Varga, J. Ultimate load-carrying ability of rib-stiffened 2024-T3 and 7075-T6 aluminium alloy panels under axial compression. Materials 2021; 14: 1176.
10. Lu B, Fang Y, Xu DK, Chen J, Ou H, Moser NH, Cao J. Mechanism investigation of friction-related effects in single point incremental forming using a developed oblique roller-ball tool. International Journal of Machine Tools and Manufacture 2014; 85: 14-29.
11. Kumar G, Maji K. Investigations on formability of tailor laminated sheets in single point incremental forming. Journal of Engineering Manufacture 2022; 09544054221076244.
12. Cristino, VAM, Pragana, JPM, Bragança, IMF, Silva, CMA, Martins, PAF. Hybrid manufacturing of stiffening grooves in additive deposited thin parts. Journal of Manufacturing and Materials Processing 2021; 5: 140.
13. ASTM E8/E8 M. Standard Test Methods for Tension Testing of Metallic Materials; ASTM International: West Conshohocken, PA, USA, 2016.
14. Silva, MB, Nielsen, PS, Bay, N, Martins, PAF. Failure mechanisms in single-point incremental forming of metals. International Journal of Advanced Manufacturing Technology 2011; 56: 893–903.
15. Martins, PAF, Barata Marques, MJM. Plane strain rigid plastic finite element formulation for sheet metal forming processes. Journal of Engineering Manufacture 1993; 207: 167-171.
16. Marciniak, Z, Duncan, JL. The mechanics of sheet metal forming, 1st ed.; Edward Arnold, Auckland, New Zealand, 1992: 100-113.

17. Chang, ZD, Li, M, Chen, J. Analytical modeling and experimental validation of the forming force in several typical incremental sheet forming processes. International Journal of Machine Tools and Manufacture 2019; 140: 62-76.

FIGURE CAPTIONS

Figure 1 (a) Stretch forming of thin panels and strengthening by means of longitudinal (b) 'T-shape' stringers or (c) stiffening grooves.

Figure 2 True stress–strain curves of AISI 316L stainless steel sheets. The symbols P, I and T refer to the parallel, inclined, and transverse orientations against the rolling direction.

Figure 3 Schematic representation and photograph of the experimental setup to fabricate the stiffening grooves by SPIF under laboratory conditions.

Figure 4 (a) Initial and (b) final computed meshes obtained from finite element analysis.

Figure 5 (a) Cross-section of the stiffening groove with notation; (b) Area of the local contact between the tool and the sheet placed immediately ahead.

Figure 6 Experimental, numerical, and analytical evolutions of the (a) cross-sectional geometry and (b) thickness of the stiffening groove for two different instants of time corresponding to a groove depth H of the semi-hemispherical tip tool equal to 5 mm and 11 mm.

Figure 7 Principal strain space showing the experimental and finite element computed in-plane strains along the perimeter of the stiffening groove for an instant of time corresponding to a depth $H = 14$ mm immediately after cracking.

Figure 8 Force per unit of length as a function of the groove depth.

Figure 9 Experimental, numerical, and analytical evolutions of the forming tool force vs. groove depth.

Table 1. Mechanical properties of the AISI 316L stainless steel sheets.

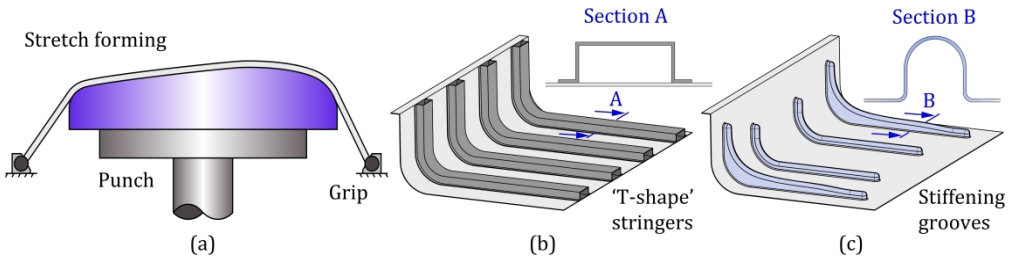

Figure 1 - (a) Stretch forming of thin panels and strengthening by means of longitudinal (b) 'T-shape' stringers or (c) stiffening grooves.

149x36mm (1200 x 1200 DPI)

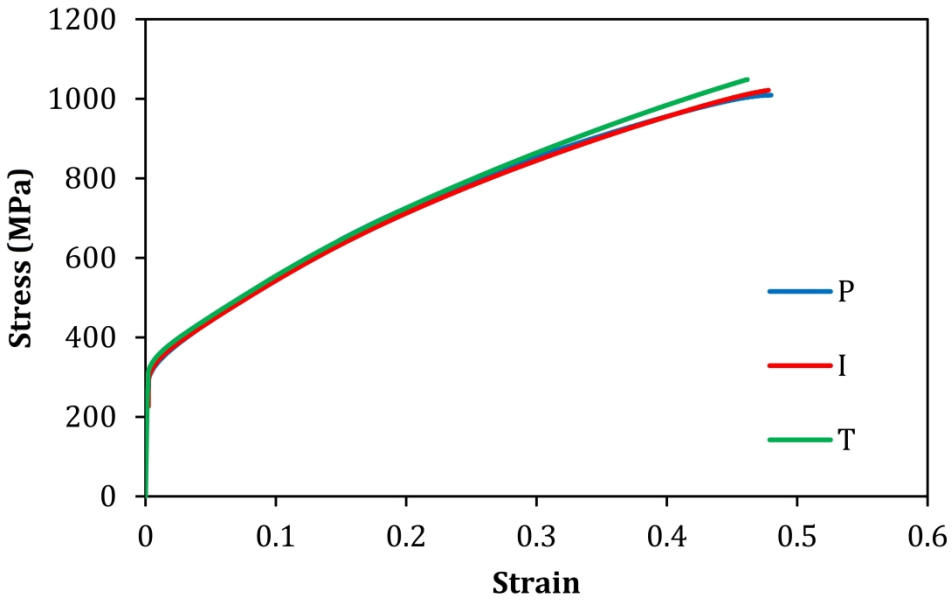

Figure 2- True stress–strain curves of AISI 316L stainless steel sheets. The symbols P, I and T refer to the parallel, inclined, and transverse orientations against the rolling direction.

111x69mm (1200 x 1200 DPI)

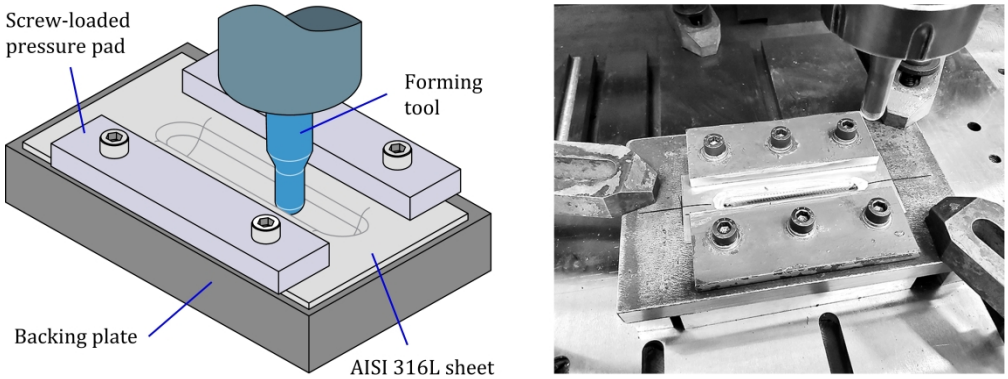

Figure 3- Schematic representation and photograph of the experimental setup to fabricate the stiffening grooves by SPIF under laboratory conditions.

147x54mm (1200 x 1200 DPI)

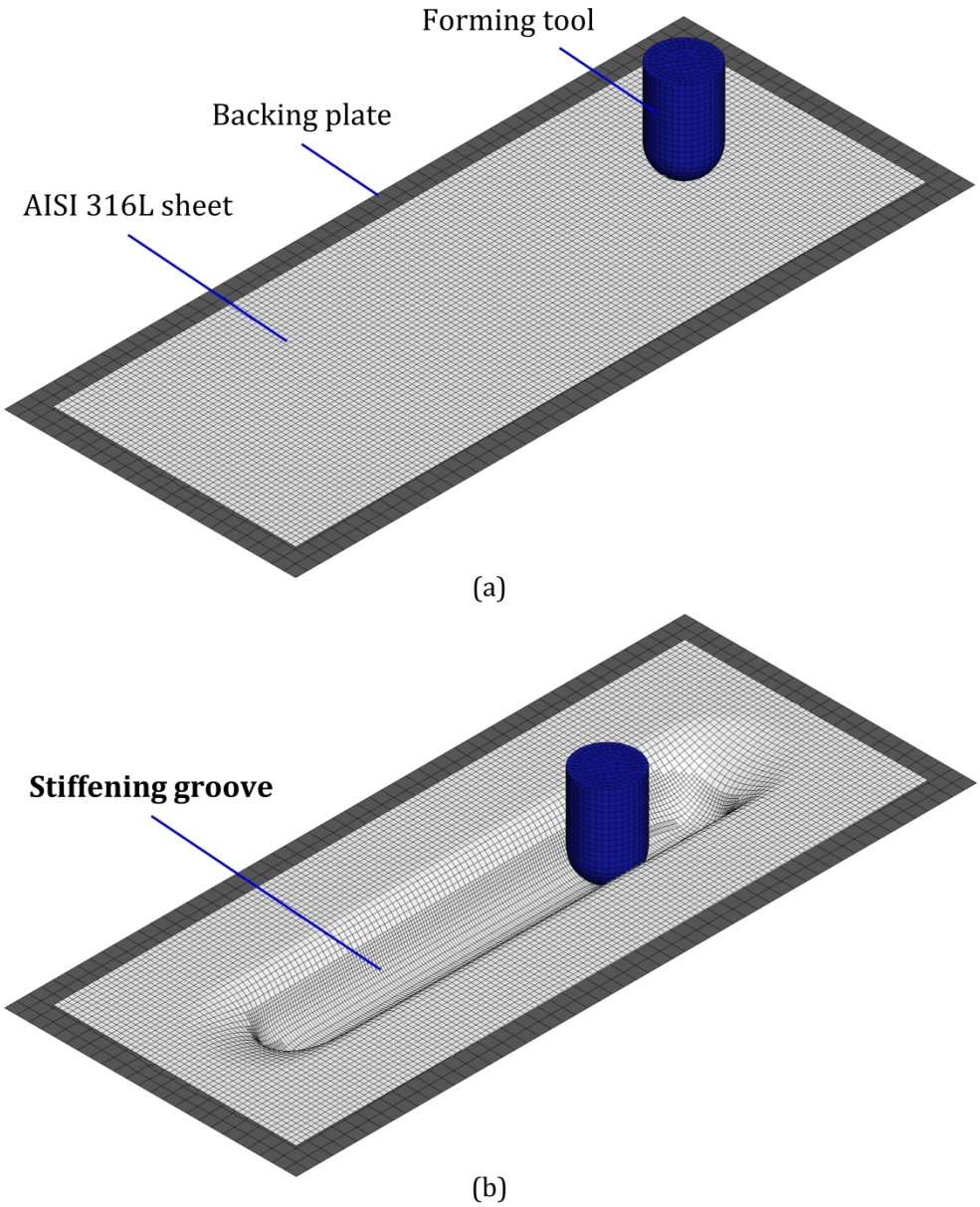

Figure 4 - (a) Initial and (b) final computed meshes obtained from finite element analysis.

110x134mm (1200 x 1200 DPI)

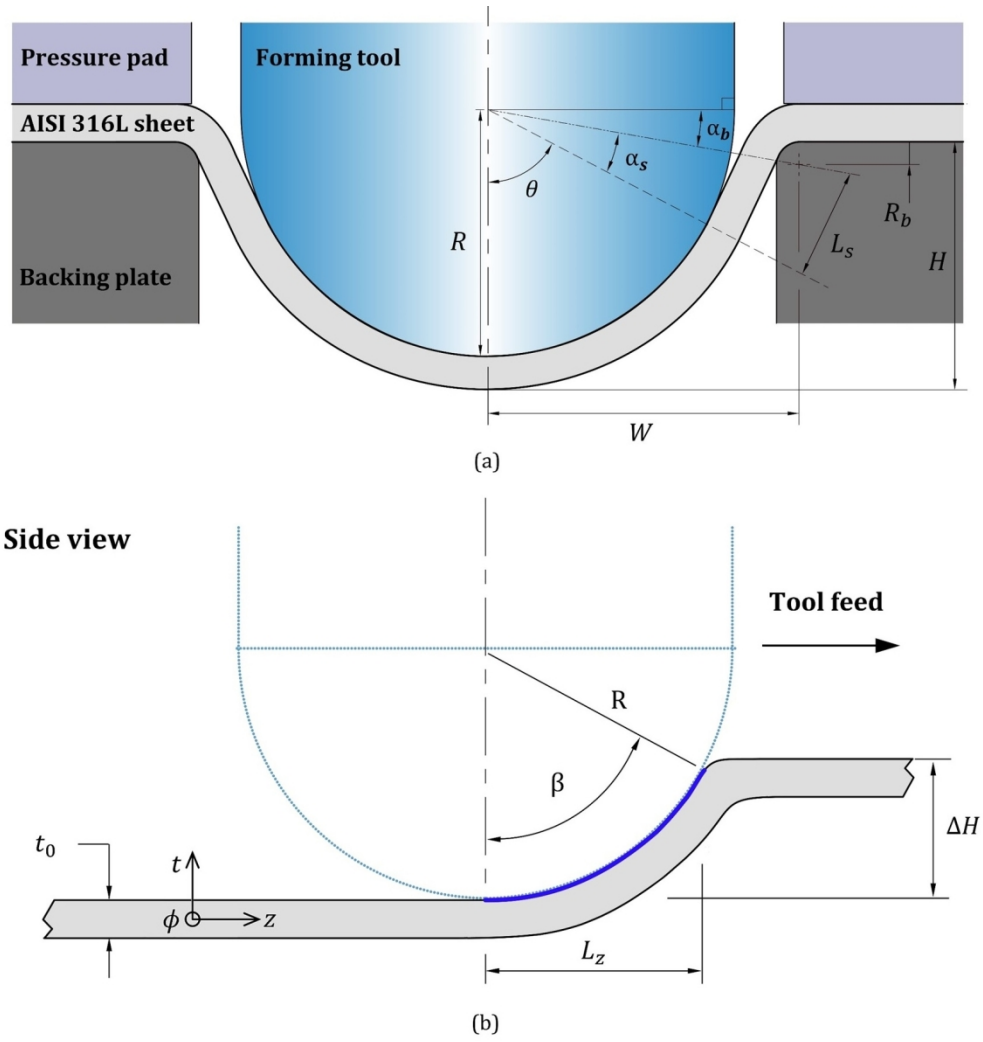

Figure 5 - (a) Cross-section of the stiffening groove with notation; (b) Area of the local contact between the tool and the sheet placed immediately ahead.

144x150mm (300 x 300 DPI)

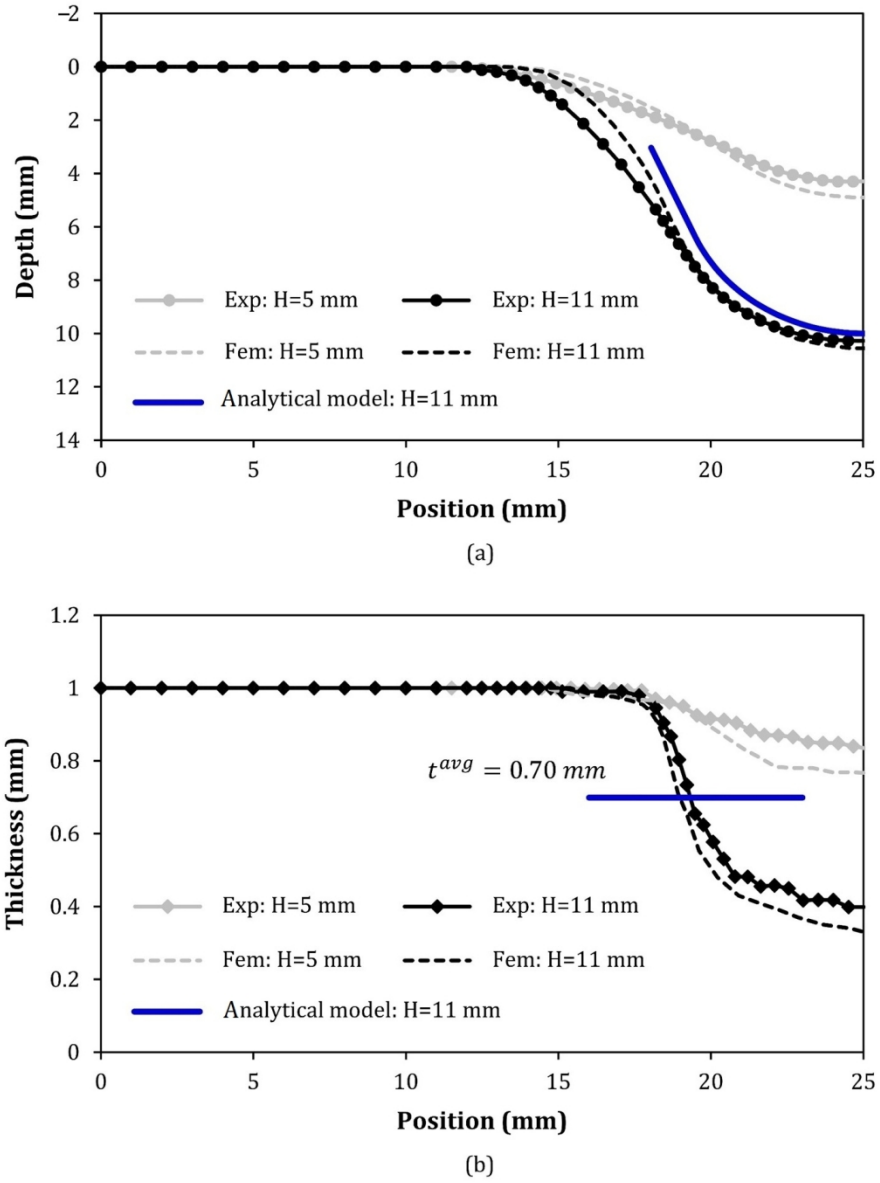

Figure 6 - Experimental, numerical, and analytical evolutions of the (a) cross-sectional geometry and (b) thickness of the stiffening groove for two different instants of time corresponding to a groove depth H of the semi-hemispherical tip tool equal to 5 mm and 11 mm.

122x163mm (300 x 300 DPI)

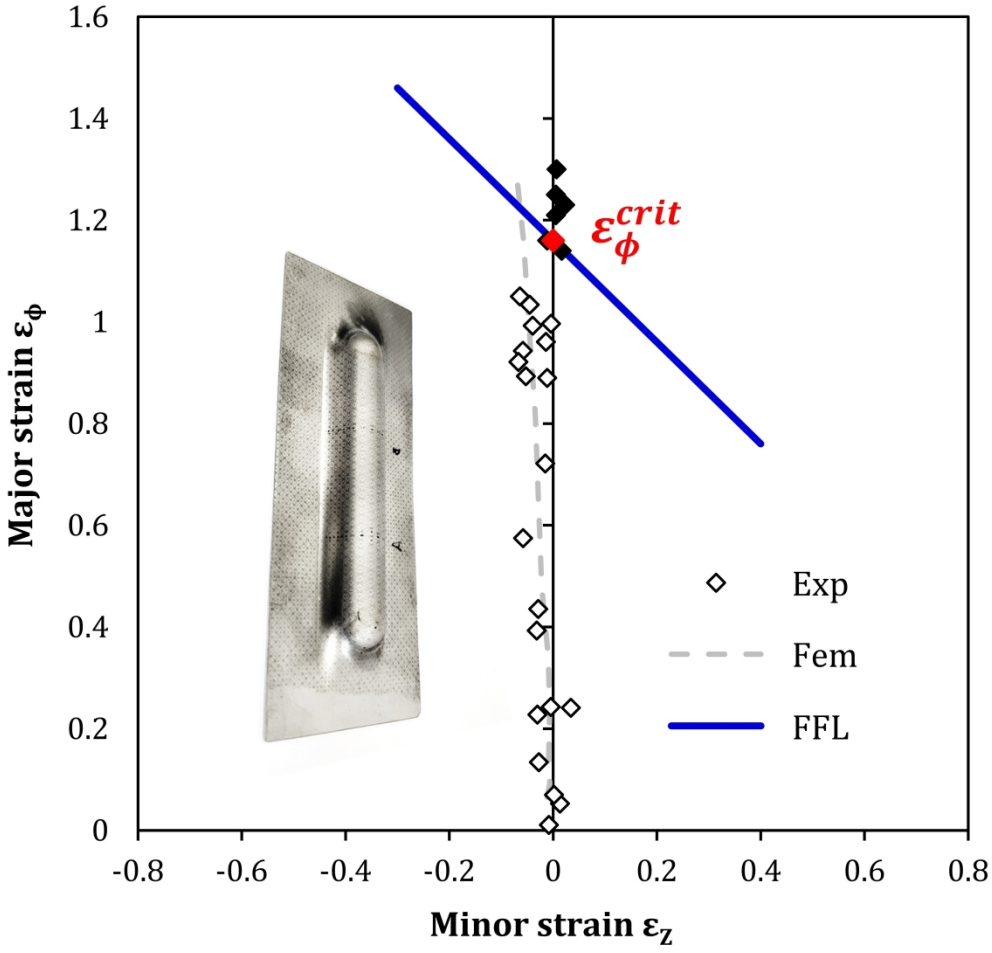

Figure 7 - Principal strain space showing the experimental and finite element computed in-plane strains along the perimeter of the stiffening groove for an instant of time corresponding to a depth H=13 mm immediately after cracking.

99x95mm (1200 x 1200 DPI)

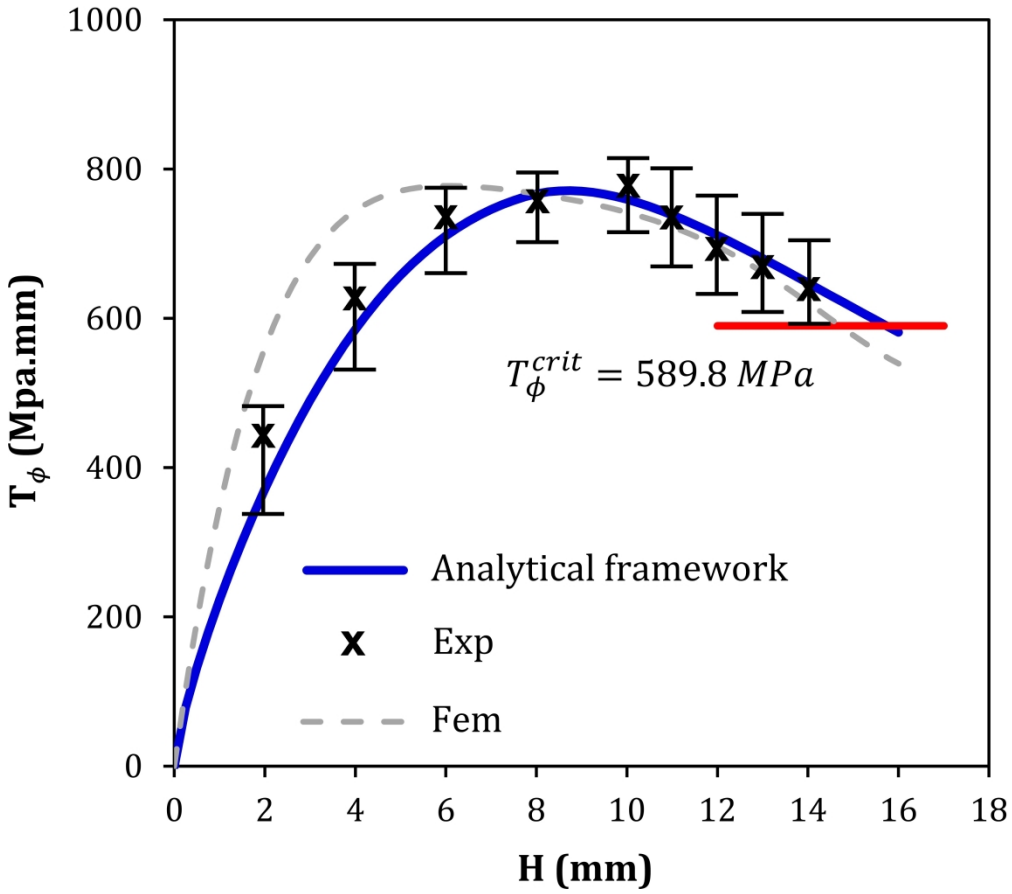

Figure 8 - Force per unit of length as a function of the groove depth.

91x80mm (1200 x 1200 DPI)

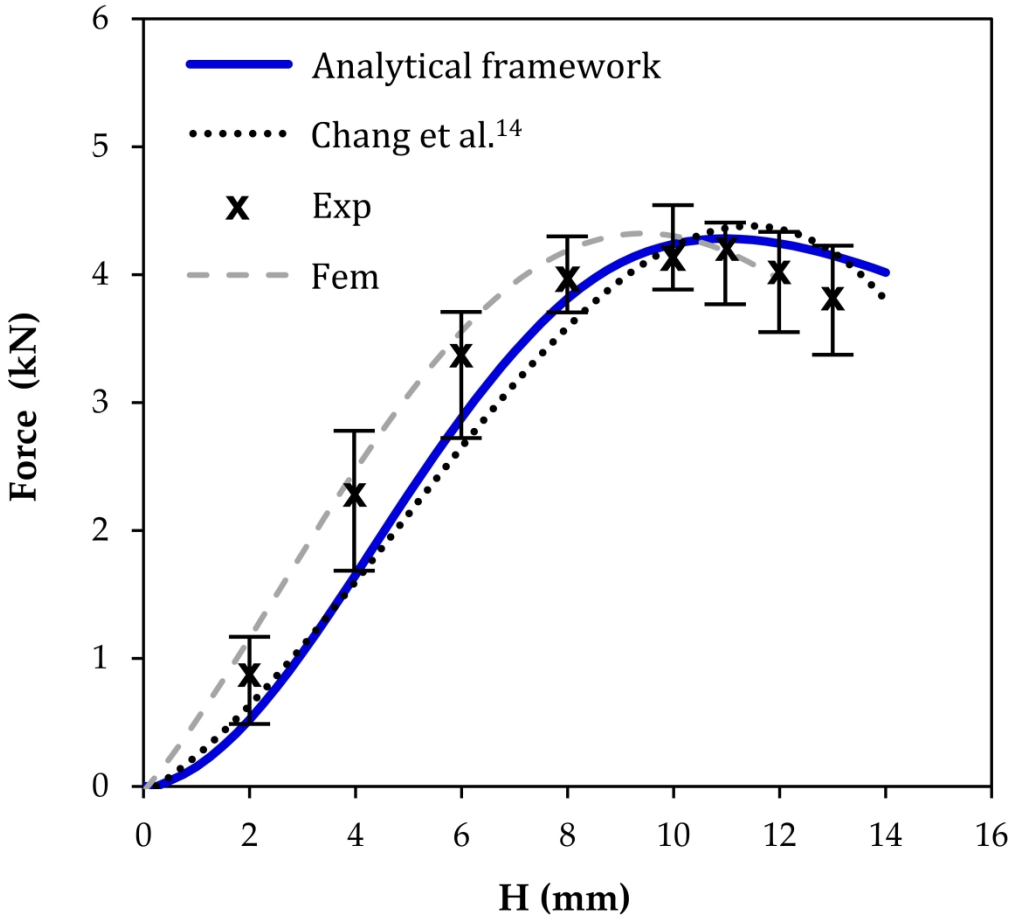

Figure 9 - Experimental, numerical, and analytical evolutions of the forming tool force vs. groove depth.

93x85mm (1200 x 1200 DPI)

Table 1. Mechanical properties of the AISI 316L stainless steel sheets.

Material	Orientation	Yield stress (MPa)	Elongation at break (%)	Anisotropy coefficient
AISI 316L	P	320.7 ± 4.4	64.9 ± 3.3	0.94
	I	313.5 ± 3.1	63.6 ± 3.5	0.97
	T	310.5 ± 3.8	61.2 ± 4.1	0.98
Average values		312.25	63.33	0.97